Synthesis of superconducting SbS and SbS_2 antimony chalcogenide compounds at high pressures

Wenting Zhang,[1] Fubo Tian,[1] Yansun Yao,[2] Xiaoli Huang,[1,*] Hui Xie,[1] Yanping Huang,[3] Defang Duan,[1] and Tian Cui[1,3,†]

[1]*State Key Laboratory of Superhard Materials, College of Physics, Jilin University, Changchun 130012, China*

[2]*Department of Physics and Engineering Physics, University of Saskatchewan, Saskatoon, Saskatchewan, Canada, S7N 5E2*

[3]*School of Physical Science and Technology, Ningbo University, Ningbo 315211, China*

(Received 21 September 2020; revised 25 February 2021; accepted 1 March 2021; published 10 March 2021)

New functional materials based on chalcogenides have promising significant applications spanning from field-effect transistors to electronic and optovalleytronic devices, and even to superconductivity. Here we report two chalcogenide materials SbS and SbS_2, obtained in pressure-induced decomposition of Sb_2S_3 at 26.3 GPa. Different from the semiconducting Sb_2S_3 precursor, both SbS and SbS_2 compounds are metallic at high pressure. Superconducting state is observed in the decomposed sample above 42 GPa, signified by a sharp drop of the resistance to zero upon cooling and a decrease of the transition temperature with the external magnetic field. Through diffraction data, SbS is determined as a major component responsible for superconductivity. The measured T_c has a nearly linear increase with applied pressure, *i.e.*, $dT_c/dP \sim 0.1\,\mathrm{K\,GPa^{-1}}$, which reaches 6.6 K at 75.0 GPa. The experimental T_c values are in general agreement with the calculation based on BCS theory, but the trend with pressure is reversed, indicating the abnormal superconducting behavior in SbS. The present results expand the chalcogenide family with two members and also open an avenue in finding the acquisition of superconducting materials in this group.

DOI: 10.1103/PhysRevB.103.104102

I. INTRODUCTION

Design and manufacture of new materials with targeted properties are driving forces for modern technology. A successful material design requires insights into fundamental principles that dictate the properties of interest, and finding the physical systems that can capture those properties. Often times, new materials are obtained by manipulating existing materials subject to changes such as chemical composition, dimensionality, and geometric size. In this field, external pressure is an efficient tool to modify or synthesize materials by accessing new states of matter that cannot be reached at ambient conditions [1–4]. For decades, high-pressure methods based on diamond-anvil cells have produced many critical new materials. Examples of high-pressure materials include new alkaline earth/transition-metal nitrides [5,6], hydrogen-rich metal hydrides [7–10], and unusual stoichiometric sodium chlorides [11]. Among these, the recent discovery of high-temperature superconductivity in binary H_3S [12,13] and LaH_{10} [14,15] marks a milestone for high-pressure synthesis, which sparks a new "gold rush" in superconductivity.

Main-group metal trichalcogenides A_2B_3 (A = Sb, Bi; B = S, Se, Te) have attracted considerable interest due to their unique thermoelectric and optoelectronic properties [16,17]. Under high pressure, A_2B_3 compounds are prone to structural changes with emergence of new/enhanced properties [18–20]. In Bi_2Te_3 and Sb_2Te_3, topological superconductivity was likely realized [21,22], and thermoelectric properties drastically enhanced by application of external pressure [16,17]. A combined theory-experiment study discovered that Bi_2Te_3 will develop into a Bi-Te substitutional solid solution at pressures above 14 GPa [18]. Sb_2S_3 has outstanding thermoelectric properties which are seeing bright prospect for applications in photovoltaic cells, gas sensors, and thermoelectric cooling devices [23,24]. At ambient conditions, Sb_2S_3 crystallizes in *Pnma* structure [25] and has the widest band gap ($E_g \sim 1.7$ eV) in the A_2B_3 group. Under high pressure, Sb_2S_3 undergoes reconstructive phase transitions, electronic topological transitions, and insulator-metal transitions [26–29]. Albeit extensive studies, no other stoichiometries than Sb_2S_3 have been found in high-pressure experiments, which is against the intuition that binary compounds should become more multistoichiometric under high pressure.

Here we report two stoichiometries, SbS and SbS_2, realized experimentally and confirmed by density-functional theory (DFT) calculations at high pressure. The realization of these two compounds is a bit unusual—they are obtained as the decomposition products of Sb_2S_3 under high pressure, rather than from a reactive synthesis. Significantly, they have interesting bonding and electronic properties, and exhibit superconductivity at high pressure with SbS being the major component. The measured T_c has a nearly linear increase with pressure, and possible reasons for this phenomenon are addressed.

II. RESULTS AND DISCUSSION

Before high-pressure experiment, purity and crystal structure of Sb_2S_3 sample were confirmed by using

*huangxiaoli@jlu.edu.cn
†cuitian@nbu.edu.cn

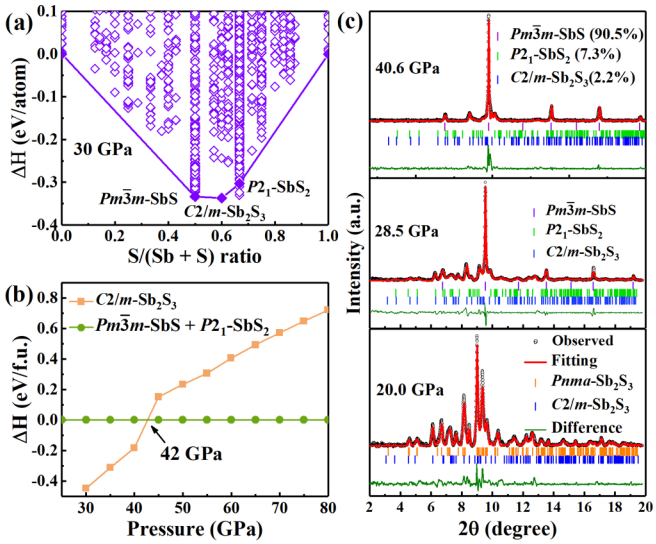

FIG. 1. Enthalpy and XRD patterns of Sb-S system under high pressure. (a) Calculated convex hull for Sb-S system at 30 GPa. (b) Calculated enthalpy difference of $C2/m$-Sb_2S_3 as a function of pressure, and the combined enthalpy of $Pm\bar{3}m$-SbS and $P2_1$-SbS_2 is used as the reference energy. (c) Full-profile experimental XRD patterns for Sb-S system at various pressures. The x-ray wavelength is 0.4064 Å.

x-ray-diffraction (XRD) measurements (Fig. S1 [30]). The ambient structure is confirmed as the orthorhombic *Pnma* structure with lattice parameters $a = 11.299$ Å, $b = 3.833$ Å, and $c = 11.222$ Å. This is followed by *in situ* high-pressure XRD measurements to detect the structural changes in Sb_2S_3 (Fig. S2 [30]). At 13.9 GPa, the first phase transition takes place, shown by the appearance of additional Bragg peaks. By comparing the XRD patterns with the reported literature [26], we identify the phase as previously reported high-pressure phase: $C2/m$-Sb_2S_3. The dynamic stability of $C2/m$-Sb_2S_3 is established by the calculated phonon dispersion relations at 20 GPa (Fig. S3 [30]). At 26.3 GPa, another phase emerges in the XRD pattern. All peaks for this phase can be unambiguously indexed to a bcc lattice (space group: $Im\bar{3}\ m$). Initially, we attempted to interpret the *bcc* lattice to a substitutional solid solution of Sb_2S_3 following previous suggestion [26], but to do so the unit-cell volume of Sb_2S_3 would have to anomalously expand to 103.29 Å^3 at 26.3 GPa. The enormous volume mismatch suggests that the structure may have a different composition. To verify this on theoretical grounds, we carried out variable-composition crystal structure searches for the Sb-S system at 30 GPa [Fig. 1(a)]. The obtained convex hull shows that SbS, SbS_2, and Sb_2S_3 are all stable stoichiometries at this pressure, suggesting the possibility for Sb_2S_3 to decompose as $Sb_2S_3 \rightarrow SbS+SbS_2$. Furthermore, enthalpy calculation shows that the physical mixture of SbS and SbS_2 in $Pm\bar{3}m$ and $P2_1$ structures, respectively, are thermodynamically more stable than $C2/m$-Sb_2S_3 above 42 GPa [Fig. 1(b)]. Calculated phonon dispersion relations also show that both $Pm\bar{3}m$-SbS and $P2_1$-SbS_2 are dynamically stable (Fig. S4 [30]). An important point to note for this decomposition is that $Pm\bar{3}m$-SbS has a bcc lattice, which is consistent with the experimental XRD pattern.

To this end, full-profile refinement of the XRD pattern measured at selected pressures was performed using the predicted structures [Fig. 1(c)]. At 20.0 GPa, the experimental XRD pattern is interpreted as the coexistence of $Pnma$-Sb_2S_3 and $C2/m$-Sb_2S_3. The diffraction pattern at 28.5 GPa is fitted to a physical mixture of $Pm\bar{3}m$-SbS, $P2_1$-SbS_2, and $C2/m$-Sb_2S_3. Note that for SbS_2, there are four other structures having lower enthalpies than $P2_1$-SbS_2 [Fig. 1(a)], but none matches the diffraction lines. Above 26.3 GPa, the Bragg peaks from $Pm\bar{3}m$-SbS become progressively pronounced, while those from $C2/m$-Sb_2S_3 and $P2_1$-SbS_2 both reduce in intensity (Fig. S2 [30]). By 40.6 GPa, the sample is primarily of $Pm\bar{3}m$-SbS with a small residue of Sb_2S_3 and $P2_1$-SbS_2 [Fig. 1(c)]. By refining the diffraction pattern at 40.6 GPa, the volume fractions of each component in the sample are approximately determined as 90.5% SbS, 7.3% SbS_2, and 2.2% Sb_2S_3, which corresponds to the following decomposition route:

$$Sb_2S_3 \rightarrow 1.77\ SbS + 0.814\ S + 0.043\ Sb_2S_3 + 0.144\ SbS_2.$$

The diffraction signal from elemental sulfur was not observed due to its amorphous states at this pressure [44,45]. The calculated enthalpy difference of the physical mixture of four substances relative to Sb_2S_3 further establishes the possibility of the decomposition path (Fig. S5 [30]). Therefore, both experimental and theoretical results converge to the conclusion that at high pressure Sb_2S_3 decomposes into chalcogenides $Pm\bar{3}m$-SbS and $P2_1$-SbS_2, which cause the changes in XRD pattern and abnormal volume expansion.

The refined structural parameters of $Pm\bar{3}m$-SbS and $P2_1$-SbS_2 are presented in Table S1 and their crystal structures can be found in Fig. S6 [30]. $P2_1$-SbS_2 has a primitive monoclinic unit cell with four formula units. This structure has seven-coordinated atom arrangement formed by edge-sharing SbS_7 decanedra. $Pm\bar{3}m$-SbS has a prototypic CsCl structure, while the atomic coordination is eight. Experimental *P-V* data and lattice parameters for $Pnma$-Sb_2S_3, $C2/m$-Sb_2S_3, $Pm\bar{3}m$-SbS, and $P2_1$-SbS_2 are obtained at various pressures (Figs. S7 and S8 [30]). Upon decompression, $Pm\bar{3}m$-SbS and $P2_1$-SbS_2 remain metastable at pressures as low as 26 GPa and transform back to the original $Pnma$-Sb_2S_3 (Figs. S2 and S9 [30]) at ambient conditions. In addition, a previous experimental study by Akahama *et al.* has shown the recrystallization and reorientation of elemental sulfur at 54.5 GPa [45]. In our experimental XRD results in run 2 (Figs. S9 and S10), elemental sulfur could also be traced in the sample. Besides, formation enthalpy calculations show that $Pnma$-Sb_2S_3 is the only stable composition at ambient conditions, consistent with experimental results and validating our theoretical method adopted here (Fig. S11 [30]).

To investigate the electronic properties and superconductivity, high-pressure variable-temperature electrical resistance measurements were carried out on the compressed Sb_2S_3. The scheme of apparatus for four-probe electrical resistance measurement is shown in Fig. 2(a). We have measured *R-T* curve at different pressures (see Fig. 2(b) and Fig. S12 [30]). The measured resistance at 75 GPa is reduced by five orders of magnitude. Characteristic metal behaviors, i.e., low resistance at low temperatures and nearly linear increase of resistivity with temperature above about 100 K, are observed at

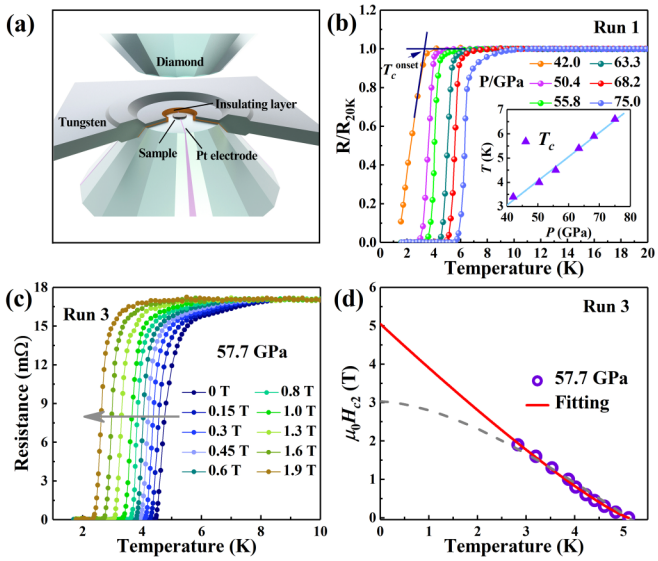

FIG. 2. Pressure-induced superconductivity in compressed Sb_2S_3 sample. (a) Schematic diagram of the setup for four-probe electrical resistance measurements. (b) Temperature-dependent resistance relative to the value at 20 K measured at different pressures. Inset: T_c derived at different pressures (triangles) and its linear fit (line). (c) Measured resistance as a function of temperature with different magnetic field at 57.7 GPa in run 3. (d) Dependence of T_c on external magnetic field H_c. Circles indicate T_c at different magnetic fields. Solid line in red represent fitting results by equation $H_{c2}(T) = H_{c2}(0)(1-\frac{T}{Tc})^{1+\alpha}$. Dashed line in gray indicate fitting result by WHH equation.

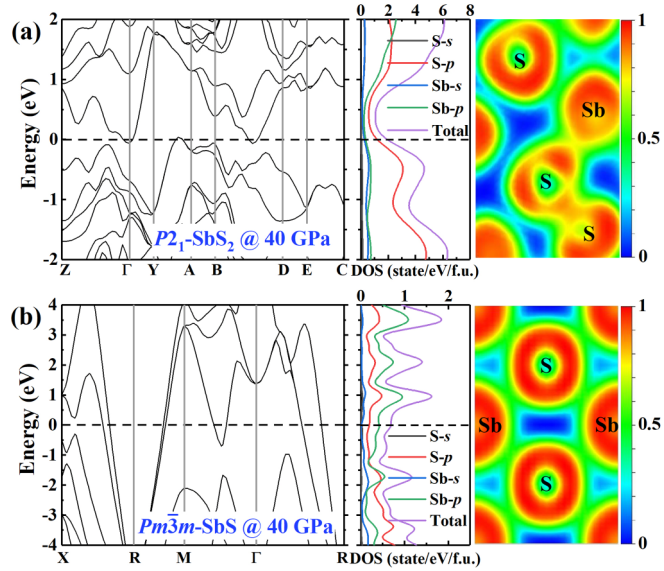

FIG. 3. Calculated electronic properties of SbS_2 and SbS at 40 GPa. Calculated band structure, DOS, and ELF for (a) $P2_1$-SbS_2 and (b) $Pm\bar{3}m$-SbS at 40.0 GPa. The dashed line indicates the Fermi level.

36.0 GPa (Fig. S12(a) [30]). This pressure-induced metallization is consistent with previous report [27]. At 42.0 GPa, the first sharp resistance drop as the manifestation of superconductivity is observed [Fig. 2(b)]. The determined superconducting critical temperature T_c (crossing point of the resistance slopes before and after the transition) is about 3.4 K. At this pressure, however, zero resistance is not yet achieved to at least 1.5 K, the lowest temperature attempted in the experiment. Until 50.4 GPa, the resistance clearly drops to zero with $T_c \sim 4$ K, showing a firmly established superconducting state. Similar resistance drop at increased T_c can be tracked up to 75.0 GPa, the highest pressure attempted in experimental run 1. Above 50.4 GPa, the superconducting transition is quite sharp, indicating good homogeneity of the superconducting phase. The measured T_c among 42.0–75.0 GPa has a nearly linear relation to the pressure [Fig. 2(b), inset], with the slope $dT_c/dP \sim 0.1\,\mathrm{K\,GPa^{-1}}$. In the second run, we have reproduced the superconducting transition and linear increment of T_c up to 87.2 GPa (Fig. S13 [30]).

To confirm the superconducting state, we also measured resistance with different magnetic field at 57.7 GPa [Fig. 2(c)]. T_c shifts to lower temperatures when the applied magnetic field (H_c) is increased to 1.9 T. The H_c versus T_c relation at 57.7 GPa further validates the superconducting state in Sb-S compounds [Fig. 2(d)], deviating from the Werthamer-Helfand-Hohenberg (WHH) equation based on the single-band model [46]. The upper critical field of the sample has a positive curvature in the vicinity of T_c. Our experimental value of $H_{c2}(T)$ was extrapolated using $H_{c2}(T) = H_{c2}(0)(1-\frac{T}{Tc})^{1+\alpha}$ equation [47]. The equation yielded $H_c(0)$ as 5.1 T. We also conducted the electrical resistance measurement during the pressure release (Figs. S14 and S15 [30]). The T_c is suppressed to lower temperatures with decreasing the pressure and increasing the external magnetic field. The superconductivity is sustained upon decompression to 35.0 GPa.

The calculated band structure and density of states (DOS) using DFT method show that both $P2_1$-SbS_2 and $Pm\bar{3}m$-SbS are metallic, revealed by considerable DOS at the Fermi level [Figs. 3(a) and 3(b)]. In the vicinity of the Fermi level, the majority of the electronic states is originated from the S-p orbitals in $P2_1$-SbS_2 and Sb-p orbitals in $Pm\bar{3}m$-SbS. The metallic nature of these two phases is consistent with the present electrical resistance measurement. The electron localization function (ELF) was also calculated to examine the bonding nature in these two compounds. For $P2_1$-SbS_2, electron localization between Sb and S atoms (ELF $\sim$ 0.75) corresponds to weak covalent bonds, while that between S and S atoms (ELF–0.85) suggests stronger covalent bonds. In $Pm\bar{3}m$-SbS, the ELF value close to 0.6 between Sb and S atoms corresponds to delocalized electrons and this leads to strong metallicity, which establishes the relation between emergence of metallicity and free-electron gas in specific bcc configuration. Both $P2_1$-SbS_2 and $Pm\bar{3}m$-SbS phases have unique bonding characteristics, distinctly different from the layered $Pnma$-Sb_2S_3 and Bi_2Te_3 [48,49].

From experimental XRD and superconductivity data, 90% percent of the product after decomposition is $Pm\bar{3}m$-SbS at 40.6 GPa, along with a small amount of SbS_2, $C2/m$-Sb_2S_3 and S [Fig. 1(c)]. Thus, theoretical investigation on superconducting properties is focused on $Pm\bar{3}m$-SbS. The projected phonon densities of states (PHDOS), Eliashberg spectral function $\alpha^2F(\omega)$, and electron-phonon coupling (EPC) integral λ

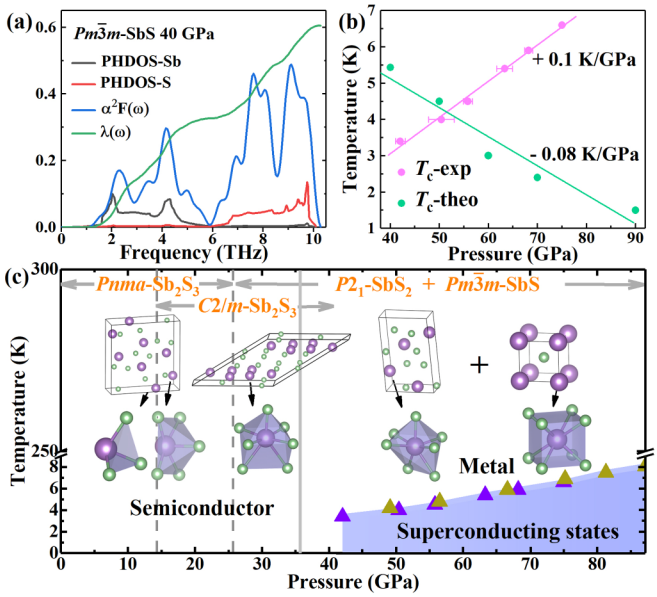

FIG. 4. Calculated superconducting properties of $Pm\bar{3}m$-SbS and experimental phase diagram of Sb-S compounds. (a) Projected phonon densities of states, Eliashberg spectral function, and the EPC strength for $Pm\bar{3}m$-SbS at 40 GPa. (b) Experimental (pink dots with error bars) and calculated (green dots) T_c of $Pm\bar{3}m$-SbS under different pressures. (c) Phase diagram of Sb-S compounds under pressure. The large violet and small green spheres in the crystal structures represent Sb and S atoms, respectively. The triangles in violet and yellow are the values of T_c obtained in experimental run 1 and run 2 respectively.

for $Pm\bar{3}m$-SbS at 40 GPa were calculated [Fig. 4(a) and Fig. S16 [30]]. The calculated λ is 0.60 and the logarithmic average phonon frequency $\omega_{\log}$ obtained from the PHDOS is 232 K. T_c was obtained using the Allen-Dynes-modified McMillan formula [50] with the nominal value of Coulomb pseudopotential μ^* ($\mu^* = 0.1$). EPC calculation yields an estimated T_c of 5.4 K for $Pm\bar{3}m$-SbS at 40 GPa, which is comparable to the experimental value [~3.8 K at 40 GPa, Fig. 2(b), inset]. The low-frequency vibrational modes dominated by Sb and high-frequency ones by S contribute nearly equally to the integral $\lambda(\omega)$. Calculation shows that in $Pm\bar{3}m$-SbS, T_c should decrease slowly in the pressure range of 40–90 GPa with the slope $dT_c/dP \sim -0.08\,\mathrm{K\,GPa^{-1}}$ [Fig. 4(b)]. The calculated superconducting parameters of $Pm\bar{3}m$-SbS as functions of pressure are provided in Fig. S17 [30]. Both λ and DOS at the Fermi level $N(E_f)$ decrease with pressure, and therefore a decrease in calculated T_c. Again the theoretical T_c values are comparable to the experimental values but the trend with pressure is opposite. To confirm the origin of superconductivity measured, we also performed the electrical resistance measurements on pure Sb (Fig. S18 [30]). The zero-electrical resistance was observed at 7.7 GPa but the T_c of Sb was suppressed with elevated pressure and vanished above 31.5 GPa, in agreement with the previous work [51,52].

For elemental sulfur, pressure-induced superconductivity was observed by Shimizu *et al.* with $T_c \sim 12$ K between 80 and 100 GPa [53,54], Struzhkin *et al.* observed that sulfur transformed into a superconductor above 93 GPa with a starting T_c of 10.1 K [55]. In another work, superconductivity of sulfur was detected above 90 GPa, with the peak characteristic of superconducting transition at 93 GPa, and observed T_c of 10–12 K [56]. Thus, the superconductivity of the compressed Sb_2S_3 sample was deemed to mainly come from $Pm\bar{3}m$-SbS.

Figure 4(c) illustrates the phase diagram of compressed Sb_2S_3 discovered in this work. This set of Sb-S compounds have diverse crystal structures. In polyhedral view, *Pnma*-Sb_2S_3 contains SbS_3 tetrahedra and SbS_5 square pyramids; $C2/m$-Sb_2S_3 has SbS_7 octahedra; $P2_1$-SbS_2 has SbS_7 decanedra; and $Pm\bar{3}m$-SbS has SbS_8 cubes. With increasing the pressure, the crystal structure breaks and evolves to more compacted structures with higher coordination, and ends at a bcc structure. Generally, in conventional phonon-mediated superconductors (such as MgB_2), T_c usually decreases with elevated pressure due to phonon stiffening. However, compounds in the A_2B_3 family have very complex pressure dependences of T_c [21,22,57,58]. Pressure evolution of T_c in Bi_2Te_3 exhibits a notable suppression after it reaches a maximum value [57]. In contrast, T_c of Bi_2Se_3 increases from its onset at 11 GPa to the peak at 30 GPa, and then stays essentially constant [58]. In Sb_2S_3, the obtained T_c increases monotonically to the highest pressure, the onset pressure (42 GPa) is consistent with the decomposition $Sb_2S_3 \rightarrow SbS + SbS_2$, and the superconductivity is originated from SbS [Fig. 1(c)].

III. CONCLUSIONS

In conclusion, two compounds $Pm\bar{3}m$-SbS and $P2_1$-SbS_2 were discovered in pressure-induced decomposition of Sb_2S_3, with the crystal structures determined by combined theoretical structure prediction and high-pressure XRD measurements. Different from semiconducting precursor Sb_2S_3, both $Pm\bar{3}m$-SbS and $P2_1$-SbS_2 are found metallic. Furthermore, both electrical resistance and external magnetic experiments reveal that $Pm\bar{3}m$-SbS has a superconducting state at low temperature. The measured T_c exhibits a nearly linear increase with respect to the pressure, starting at about 3.4 K at 42.0 GPa and ending with 6.6 K at 75 GPa. These findings expand the stoichiometries of Sb-S system and provide insights for experimental search of novel superconductors.

ACKNOWLEDGMENTS

This work was supported by the National Key R&D Program of China (Grant No. 2018YFA0305900), National Natural Science Foundation of China (Grants No. 11974133, and No. 51720105007). Program for Changjiang Scholars and Innovative Research Team in University (Grant No. IRT_-15R23).

[1] R. M. Hazen, *The Diamond Makers* (Cambridge University Press, Cambridge, 1999).

[2] H. Fujihisa, Y. Fujii, K. Takemura, and O. Shimomura, J. Phys. Chem. Solids **56**, 1439 (1995).

[3] N. W. Ashcroft, Phys. Rev. Lett. **21**, 1748 (1968).
[4] S. Zhang, Q. Wang, Y. Kawazoe, and P. Jena, J. Am. Chem. Soc. **135**, 18216 (2013).
[5] D. Laniel, B. Winkler, E. Koemets, T. Fedotenko, and N. Dubrovinskaia, Nat. Commun. **10**, 4515 (2019).
[6] S. Wang, X. Yu, Z. Lin, R. F. Zhang, D. He, J. Qin, J. Zhu, J. Han, L. Wang, H. Mao *et al.*, Chem. Mater. **24**, 3023 (2012).
[7] C. M. Pepin, G. Geneste, A. Dewaele, M. Mezouar, and P. Loubeyre, Science **357**, 382 (2017).
[8] X. Li, X. Huang, D. Duan, C. J. Pickard, and T. Cui, Nat. Commun. **10**, 3461 (2019).
[9] D. Zhou, D. V. Semenok, D. Duan, H. Xie, W. Chen, X. Huang, X. Li, B. Liu, A. R. Aganov, and T. Cui, Sci. Adv. **6**, eaax6849 (2020).
[10] D. V. Semenok, A. G. Kvashnin, A. G. Ivanova, V. Svitlyk, V. Y. Fominski, A. V. Sadakov, O. A. Sobolevskiy, V. M. Pudalov, I. A. Troyan, and A. R Oganov, Mater. Today **33**, 36 (2020).
[11] W. Zhang, A. R. Oganov, A. F. Goncharov, Q. Zhu, S. E. Boulfelfel, A. O. Lyakhov, E. Stavrou, M. Somayazulu, V. B. Prakapenka, and Z. Konopkova, Science **342**, 1502 (2013).
[12] A. P. Drozdov, M. I. Eremets, I. A., Troyan, V. Ksenofontov, and S. I. Shylin, Nature (London) **525**, 73 (2015).
[13] M. Einaga, M. Sakata, T. Ishikawa, K. Shimizu, M. I. Eremets, A. P. Drozdov, I .A. Troyan, N. Hirao, and Y. Ohishi, Nat. Phys. **12**, 835 (2016).
[14] A. P. Drozdov, P. P. Kong, V. S. Minkov, S. P. Besedin, M. A. Kuzovnikov, S. Mozaffari, L. Balicas, F. F. Balakirev, D. Graf, V. B. Prakapenka *et al.*, Nature (London) **569**, 528 (2019).
[15] M. Somayazulu, M. Ahart, A. K. Mishra, Z. M. Geballe, M. Baldini, Y. Meng, V. V. Struzhkin, and R. J. Hemley, Phys. Rev. Lett. **122**, 027001 (2019).
[16] S. V. Ovsyannikov, V. V. Shchennikov, G. V. Vorontsov, A. Y. Manakov, A. Y. Likhacheva, and V. A. Kulbachinskii, J. Appl. Phys. **104**, 053713 (2008).
[17] N. V. C. Shekar, D. A. Polvani, J. F. Meng, and J. V. Badding, Physica B **358**, 14 (2005).
[18] L. Zhu, H. Wang, Y. Wang, J. Lv, Y. Ma, Q. Cui, Y. Ma, and G. Zou. Phys. Rev. Lett. **106**, 145501 (2011).
[19] J. Zhao, H. Liu, L. Ehm, Z. Chen, S. Sinogeikin, Y. Zhao, and G. Gu, Inorg. Chem. **50**, 11291 (2011).
[20] R. Vilaplana, D. Santamaria-Perez, O. Gomis, F. J. Manjon, J. Gonzalez, A. Segura, A. Munoz, P. Rodriguez-Hernandez, E. Perez-Gonzalez, V. Marin-Borras *et al.*, Phys. Rev. B **84**, 184110 (2011).
[21] J. Zhang, S. J. Zhang, H. Weng, W. Zhang, L. X. Yang, Q. Liu, S. M. Feng, X. C. Wang, R. Yu, L. Z. Cao *et al.*, Proc. Natl Acad. Sci. **108**, 24 (2011).
[22] J. Zhu, J. Zhang, P. P. Kong, S. Zhang, X. H. Yu, J. Zhu, Q. Liu, X. Li, R. Yu, R. Ahuja *et al.*, Sci. Rep. **3**, 2016 (2013).
[23] S. Moon, Y. Itzhaik, J. Yum, S. M. Zakeeruddin, G. Hodes, and M. Gratzel, J. Phys. Chem. Lett. **1**, 1524 (2010).
[24] M. R. Filip, C. E. Patrick, and F. Giustino, Phys. Rev. B: Condens. Matter Mater. Phys. **87**, 205125 (2013).
[25] D. O. McKee and J. T. McMullan, Z. Kristallogr. Cryst. Mater. **142**, 447 (1975).
[26] Y. Wang, Y. Ma, G. Liu, J. Wang, Y. Li, Q. Li, J. Zhang, Y. Ma, and G. Zou, Sci. Rep. **8**, 14795 (2018).
[27] L. Dai, K. Liu, H. Li, L. Wu, H. Hu, Y. Zhuang, L. Yang, C. Pu, and P. Liu, Phys. Rev. B **97**, 024103 (2018).
[28] Y. A. Sorb, V. Rajaji, P. S. Malavi, U. Subbarao, P. Halappa, S. C. Peter, S. Karmakar, and C. Narayana, J. Phys.: Condens. Matter **28**, 015602 (2016).
[29] I. Efthimiopoulos, C. Buchan, and Y. Wang, Sci. Rep. **6**, 24246 (2016).
[30] See Supplemental Material at http://link.aps.org/supplemental/10.1103/PhysRevB.103.104102 for experimental and computational methods, data pertaining to high-pressure XRD analysis and electrical resistance measurements, calculated superconducting parameters of *Pm*3*m*-SbS, which includes Refs. [31–43].
[31] C. Prescher and V. B. Prakapenka, High Pressure Res. **35**, 223 (2015).
[32] H. M. Rietveld, J. Appl. Crystallogr. **2**, 65 (1969).
[33] V. Petříček, M. Dušek, and L. Palatinus, Z. Kristallogr. Cryst. Mater. **229**, 345 (2014).
[34] B. H. Toby, J. Appl. Crystallogr. **34**, 210 (2001).
[35] H. K. Mao, J. Xu, and P. M. Bell, J. Geophys. Res. Solid Earth **91**, 4673 (1986).
[36] Y. Akahama and H. Kawamura, J. Appl. Phys. **100**, 043516 (2006).
[37] G. Kresse and D. Joubert, Phys. Rev. B **59**, 1758 (1999).
[38] G. Kresse and J. J. Furthmüller, Phys. Rev. B **54**, 11169 (1996).
[39] J. P. Perdew, K. Burke, and M. Ernzerhof, Phys. Rev. Lett. **77**, 3865 (1996).
[40] C. J. Pickard and R. J. Needs, J. Phys.: Condens. Matter **23**, 053201 (2011).
[41] A. Togo, F. Oba, and I. Tanaka, Phys. Rev. B **78**, 134106 (2008).
[42] P. Giannozzi, S. Baroni, N. Bonini, M. Calandra, R. Car, C. Cavazzoni, D. Ceresoli, G. L. Chiarotti, M. Cococcioni, I. Dabo *et al.*, J. Phys.: Condens. Matter **21**, 395502 (2009).
[43] N. Troullier and J. L. Martins, Phys. Rev. B **43**, 1993 (1991).
[44] H. Luo and A. L. Ruoff, Phys. Rev. B **48**, 569 (1993).
[45] Y. Akahama, M. Kobayashi, and H. Kawamura, Phys. Rev. B **48**, 6862 (1993).
[46] T. Baumgartner, M. Eisterer, H. W. Weber, R. Flukiger, C. Scheuerlein, and L. Bottura, Supercond. Sci. Technol. **27**, 015005 (2014).
[47] O. Pavlosiuk, D. Kaczorowski, and P. Wiśniewski, Sci. Rep. **5**, 9158 (2015).
[48] J. Ibañez, J. A. Sans, C. Popescu, J. Lopez-Vidrier, J. J. Elvira-Betanzos, V. P. Cuenca-Gotor, O. Gomis, F. J. Manjon, P. Rodríguez-Hernandez, and A. Muñoz, J. Phys. Chem. C. **120**, 10547 (2016).
[49] S. K. Mishra, S. Satpathy, and O. Jepsen, J. Phys.: Condens. Matter **9**, 461 (1997).
[50] P. B. Allen and R. C. Dynes, Phys. Rev. B **12**, 905 (1975).
[51] J. Wittig, J. Phys. Chem. Solids. **30**, 1407 (1969).
[52] K. Aoki, S. Fujiwara, and M. Kusakabe, Solid State Commun. **45**, 161 (1983).
[53] K. Shimizu, K. Amaya, and N. Suzuk, J. Phys. Soc. Jpn. **74**, 1345 (2005).
[54] S. Kometani, M. I. Eremets, K. Shimizu, M. Kobayashi, and K. Amaya, J. Phys. Soc. Jpn. **66**, 2564 (1997).

[55] V. V. Struzhkin, R. J. Hemley, H. K. Mao, and Y. A. Timofeev, Nature (London) **390**, 382 (1997).

[56] E. Gregoryanz, V. V. Struzhkin, R. J. Hemley, M. I. Eremets, H. K. Mao, and Y. A. Timofeev, Phys. Rev. B **65**, 064504 (2002).

[57] C. Zhang, L. Sun, Z. Chen, X. Zhou, Q. Wu, W. Yi, J. Guo, X. Dong, and Z. Zhao, Phys. Rev. B **83**, 140504(R) (2011).

[58] K. Kirshenbaum, P. S. Syers, A. P. Hope, N. P. Butch, J. R. Jeffries, S. T. Weir, J. J. Hamlin, M. B. Maple, Y. K. Vohra, and J. Paglione, Phys. Rev. Lett. **111**, 087001 (2013).